

# FIAT: enabling classical and modern macroelements

PABLO D. BRUBECK, University of Oxford, UK

ROBERT C. KIRBY, Baylor University, USA

Many classical and modern finite element spaces are derived by dividing each computational cell into finer pieces. Such *macroelements* frequently enable the enforcement of mathematically desirable properties such as divergence-free conditions or  $C^1$  continuity in a simpler or more efficient manner than elements without the subdivision. Although a few modern software projects provide one-off support for particular macroelements, a general approach facilitating broad-based support has, until now, been lacking. In this work, we describe a major addition to the FIAT project to support a wide range of different macroelements. These enhancements have been integrated into the Firedrake code stack. Numerical evaluation of the new macroelement facility is provided.

## 1 INTRODUCTION

Finite element methods provide a powerful suite of tools for the numerical approximation of solutions to partial differential equations posed on  $H^1$ ,  $H(\text{curl})$ ,  $H(\text{div})$ , and other Sobolev spaces. Finite element methods have broad applicability, including in unstructured geometry, and allow general approximation orders. At the same time, realizing this theoretical flexibility presents a technical challenge to the design of general and efficient software. FIAT, the Finite element Automatic Tabulator, was first introduced some two decades ago to provide a general tool for just this purpose [Kirby 2004]. FIAT is an independent library providing a suite of cells, basis functions, and quadrature rules, usable in principle by any client. After its introduction in [Kirby 2004], it was updated to recast internal operations in terms of dense linear algebra in [Kirby 2006]. FIAT’s interaction with code generation for variational forms was pursued in papers such as [Kirby and Logg 2006; Rognes et al. 2010]. Support for constructing new elements via tensor products and other higher-order operations was developed in [McRae et al. 2016]. FInAT [Homolya et al. 2017; Kirby and Mitchell 2019] enclosed abstract syntax around FIAT, enabling code generation of structured algorithms [Homolya et al. 2018] and for nonstandard pullbacks required by the theory in [Aznaran et al. 2022; Bock et al. 2024; Kirby 2018].

Absent from the vast array of elements supported in FIAT (and most other general finite element libraries) have long been *macroelements*. Based on piecewise polynomials over some subdivision of each computational cell, such elements provide important properties with lower polynomial degree and/or fewer degrees of freedom than the pure polynomial spaces previously supported in FIAT. For example, obtaining  $C^1$  continuity on triangles with pure polynomial spaces requires at least degree five. The Argyris element uses all quintic polynomials and has 21 degrees of freedom, and the Bell element contains all quartics, many quintics, and has 18 degrees of freedom. However, the Hsieh–Clough–Tocher (HCT) macroelement [Clough and Toucher 1965] requires only 12 degrees of freedom by splitting the triangle at its barycenter and using piecewise cubics. These elements have recently been extended to higher order variants [Grošelj and Knez 2022]. Unlike Bell and Argyris, these elements do not employ second derivatives at vertices as degrees of freedom, which may motivate their use at higher order.

Macroelements also permit pointwise divergence-free approximations to incompressible flow with much lower degree than standard polynomial spaces. For example, the Scott–Vogelius pair [Brenner and Scott 2008; Scott and Vogelius 1984] discretizes the Stokes equations with conforming velocities of at least quartic degree and discontinuous pressures of one degree lower. Modulo

mild mesh restrictions, this provides a stable approximation with optimal convergence rates and pointwise divergence-free velocities. Obtaining similar results on tetrahedra requires at least hexic velocities, but the results of [Guzmán and Neilan 2018] show that on barycentrically refined simplicial meshes, it is sufficient to use polynomials with degree equal to the spatial dimension (two or three). While this approach may be implemented by modifying the given computational mesh, it may also be realized through the basis functions, defining a  $C^0$  macroelement over a split cell. Iso-type elements, where one uses a piecewise  $P_1$  space on a uniform refinement of each cell, also provide a use case for macroelements. For Stokes flow, one may replace the quadratic velocities in the Taylor–Hood pair with piecewise  $P_1$  elements using the locations of the quadratic degrees of freedom, as in Fig. 2a. Using finer refinements is known to give excellent preconditioners for high-order discretizations on quadrilateral and hexahedral meshes [Pazner et al. 2023], although it is not known how to optimally adapt this approach to simplices. Other novel elements, such as the Alfeld–Sorokina [Alfeld and Sorokina 2016] and Guzman–Neilan [Guzmán and Neilan 2018] elements, form part of a discrete complex, and are also of current research interest.

The discretization of symmetric tensors, whether in stress-based formulations of fluids or in the Hellinger–Reissner formulation of elasticity, also motivates macroelements. To obtain a non-macro, polynomial,  $H(\text{div})$ -conforming symmetric stress tensor requires the lowest-order Arnold–Winther triangle [Arnold and Winther 2002] with 24 degrees of freedom. On tetrahedra, the conforming Arnold–Awanou–Winther element [Arnold et al. 2008] has a hefty 162 degrees of freedom. Somewhat smaller but nonconforming elements are known [Arnold et al. 2014; Arnold and Winther 2003]. On the other hand, [Gopalakrishnan et al. 2024] gives a macroelement in any dimension utilizing only piecewise linear polynomials on a barycentric refinement. The two-dimensional element is conforming with 15 degrees of freedom, and the three-dimensional element only has 42.

Here, we describe a major extension of FIAT to enable a broad class of simplicial macroelements and their integration into the Firedrake project [Ham et al. 2023; Rathgeber et al. 2016]. Other high-level packages provide basic support for macroelements. For example, GetFem++ [Renard and Poulis 2020] supports iso-type elements and the HCT triangle. Freefem [Hecht 2012] does as well, although iso-type elements require constructing nested meshes. Libmesh also supports HCT and some Powell–Sabin splines [Stogner and Carey 2007]. More recently, the basix library [Scroggs et al. 2022] has enabled iso-type elements. While we are not the first to enable macroelements in finite element libraries, we believe our work goes far beyond prior attempts. In particular, FIAT now possesses a far wider suite of macroelements than are available in other libraries. We have also taken special care so that Firedrake end-users select macroelements like any other element and need not carry out extra tasks like manipulating the computational mesh or manually selecting composite quadrature rules.

The rest of the paper is organized as follows. In Section 2, we describe our general approach and a suite of macroelements enabled by the new technology. This technology is further described in Section 3, where we detail modifications to FIAT to support macroelements and necessary changes to the remainder of the Firedrake code stack to enable their seamless use. Most of these elements do not map simply via affine or Piola pullbacks, and we describe the application of the theory in [Kirby 2018] to transform the HCT elements in Section 4. Similar techniques hold for the other macroelements we have implemented. Finally, numerical results evaluating the newly-enabled elements are given in Section 5 before concluding thoughts presented in Section 6.

## 2 MACROELEMENTS

Typical finite element spaces employ functions that are piecewise polynomial over each cell in the computational domain, with some restrictions on the continuity between cells. However, macroelements require each cell to be further subdivided in some regular way, so that the functions

on each cell in the mesh are themselves piecewise polynomials. These elements typically offer attractive mathematical properties, but present additional complexity for implementation. Fig. 1 depicts several common splittings used on triangles. Many of these splitting strategies, such as the uniform split in Fig. 1a and Alfeld (also known as barycentric or Clough–Tocher splitting) in Fig. 1b are affinely invariant – splitting a reference cell and mapping it to a physical cell produces the correct splitting. The Powell-Sabin-12 split in Fig. 1d and Wang splitting in Fig. 1e may also be constructed in this way.

Certain splittings, such as the 6-way Powell-Sabin split in Fig. 1c, presents more difficulty. It is desirable to split each triangle at the incenter rather than barycenter, and then split each edge where it intersects the line connecting incenters of adjacent triangles. Following the argument in [Powell and Sabin 1977], this construction guarantees the existence of splines on general meshes, while simply using a barycentric split implies a mesh restriction. Such issues affect tetrahedra to an even greater degree. Splittings like the Worsey–Farin and Worsey–Piper splits [Lai and Schumaker 2007; Worsey and Piper 1988] also require geometrically-dependent splittings to avoid mesh restrictions and in general are quite difficult to compute. Because the use of a reference element is deeply ingrained in many general finite element codes, including Firedrake, our development concentrates on affinely-preserved splits based on barycenters.

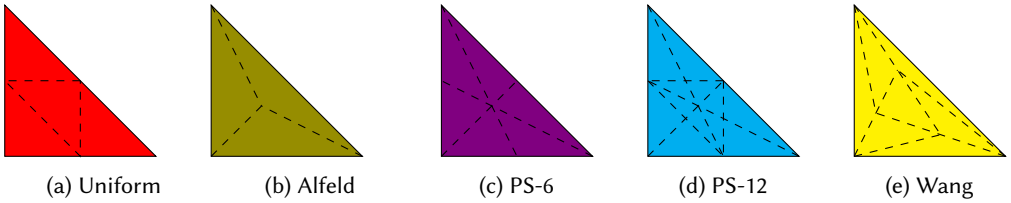


Fig. 1. Some typical splitting strategies for macroelements.

Before describing our implementation of macroelements in FIAT and the rest of the Firedrake code stack, we give a careful description of the various elements depicted above. In line with the rest of FIAT, we work in terms of the Ciarlet triple [Ciarlet 2002].

- $K \subset \mathbb{R}^d$  is a bounded domain with piecewise smooth boundary. In this paper, we only consider  $K$  as a simplex.
- $P$  is a finite-dimensional function space defined on the closure of  $K$ , typically consisting of polynomials or vectors/tensors of them, or piecewise polynomials over a subdivision of  $K$ .
- $N = \{n_i\}_{i=1}^{\dim P}$  is a basis for the dual space  $P'$ , called the set of *nodes* or *degrees of freedom*.

The *nodal basis* for a finite element is the set  $\{\phi_i\}_{i=1}^{\dim P} \subset P$  such that,

$$n_i(\phi_j) = \delta_{ij}, \quad 1 \leq i, j \leq \dim P. \quad (2.1)$$

The nodes of a finite element typically consist of functionals such as pointwise evaluation of functions or derivatives at particular points, or certain integral moments of functions on  $K$  or its boundary facets, and are chosen to enforce certain kinds of continuity between adjacent elements.

In FIAT, we compute the nodal basis numerically by means of solving a generalized Vandermonde system. Given any readily computable basis  $\{p_i\}_{i=1}^{\dim P}$  for  $P$ , we can write

$$\phi_j = \sum_{k=1}^{\dim P} A_{jk} p_k, \quad (2.2)$$

and applying any node  $n_i$  to both sides of the equation gives

$$\delta_{ij} = \sum_{k=1}^{\dim P} A_{jk} n_i(p_k), \quad (2.3)$$

so that we have

$$I = AV^\top, \quad (2.4)$$

where  $V_{ij} = n_i(p_j)$ .

Our approach represents a departure from the more commonly-used Bernstein–Bezier techniques for representing triangular splines. There are tradeoffs between the two approaches. Defining splines directly on a triangulation using Bernstein–Bezier techniques affords certain mathematical advantages, such as positive bases for some kinds of splines [Grošelj and Knez 2022] and the use of incenter splitting to avoid mesh restrictions [Powell and Sabin 1977]. When the splines are represented locally in the Bernstein basis, sum-factored algorithms can be used for finite element operators [Ainsworth et al. 2011; Kirby 2011, 2014]. However, the geometric issues become more involved in three dimensions [Lai and Schumaker 2007]. Working in terms of a reference element ties us barycentric splitting and its associated mesh restrictions, but it does give an implementation that fits squarely within the Firedrake framework. Hence, our approach gives immediate usability without major internal Firedrake redevelopment to generalize beyond the reference element paradigm.

## 2.1 Splittings

We let  $K$  be any simplex in  $\mathbb{R}^d$ . We let  $\Delta_A(K)$  be the barycentric/Alfeld split of  $K$  into  $d+1$  simplices, shown for triangles in Fig. 1b. The iso-split by  $\ell : 1$  uniform refinement will be denoted by  $\Delta_{iso,\ell}(K)$ , shown for triangles with  $\ell = 2$  in Fig. 1a. We omit the subscript when  $\ell = 2$ , so  $\Delta_{iso}(K) \equiv \Delta_{iso,2}(K)$ . For triangles, we let  $\Delta_{PS6}(K)$  and  $\Delta_{PS12}(K)$  be the sets of triangles obtained via the Powell-Sabin splits of Figs. 1c and 1d.

## 2.2 Degrees of freedom

In order to define macroelements, we need to establish some notation for degrees of freedom. For each vertex  $\mathbf{v} \in K$  of the unsplit simplex, we define the functional  $\delta_{\mathbf{v}}$  by

$$\delta_{\mathbf{v}}(p) = p(\mathbf{v}). \quad (2.5)$$

Similarly, we differentiate at  $\mathbf{v}$  in the direction of some unit vector  $\mathbf{s}$  by

$$\delta_{\mathbf{v}}^{\mathbf{s}}(p) = \mathbf{s} \cdot \nabla p(\mathbf{v}). \quad (2.6)$$

The gradient at a point is a vector of functionals

$$\nabla_{\mathbf{v}} = [\delta_{\mathbf{v}}^x \quad \delta_{\mathbf{v}}^y]^\top \quad (2.7)$$

We also need to define functionals based on integral moments over edges or faces. For any facet  $\mathbf{f}$  of  $K$  itself or its splitting and any function  $p \in L^2(\mathbf{f})$ , we define the integral moment

$$\mu_{\mathbf{f},q}(p) = \int_{\mathbf{f}} qp \, ds. \quad (2.8)$$

and for unit vector  $\mathbf{s}$  and facet  $\mathbf{f}$ , we define the integral moment of the directional derivative by

$$\mu_{\mathbf{f},q}^{\mathbf{s}}(p) = \int_{\mathbf{f}} q(\mathbf{s} \cdot \nabla p) \, ds. \quad (2.9)$$

In each of these three cases, if  $q \equiv 1$  on  $\mathbf{f}$ , we omit the subscript  $q$ . For example,

$$\mu_{\mathbf{f}}^s \equiv \mu_{\mathbf{f},1}^s(p) = \int_{\mathbf{f}} 1 (\mathbf{s} \cdot \nabla p) \, ds = \int_{\mathbf{f}} \mathbf{s} \cdot \nabla p \, ds. \quad (2.10)$$

### 2.3 $C^0$ macroelements

For any simplex  $K$ , we define the space of  $C^0$  splines of degree  $k$  over a splitting  $\Delta$  of  $K$

$$S_k^0(\Delta) = \{s \in C^0(K) : s|_{\tau} \in P_k(\tau), \tau \in \Delta\}. \quad (2.11)$$

Then, we parametrize the space by standard degrees of freedom. If  $K$  is a triangle, we choose degrees of freedom as

- $\delta_{\mathbf{v}}$  for each vertex  $\mathbf{v}$  of  $\Delta$ .
- If  $k > 1$ , take moments  $\mu_{\mathbf{e},q}$  for each edge  $\mathbf{e}$  in  $\Delta$  and each  $q$  in a basis for  $P_{k-2}(\mathbf{e})$ .
- If  $k > 2$ , take moments  $\mu_{\tau,q}$  for each  $\tau \in \Delta$  and each  $q$  in a basis for  $P_{k-3}(\tau)$ .

Alternatively (and far more commonly for low-order finite elements), one may replace the integral moments with evaluation at an appropriate set of unisolvent points. Fig. 2 shows the degree-of-freedom diagrams for some  $C^0$  macroelements.

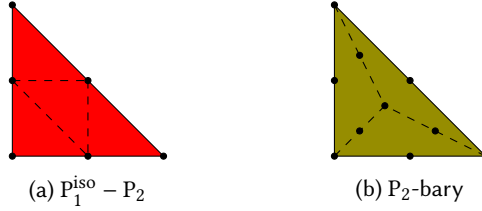


Fig. 2. Some Lagrange-type  $C^0$  macroelements. Solid dots represent point evaluation degrees of freedom.

### 2.4 $C^1$ macroelements

For  $C^1$  elements, we focus on splittings of a triangle  $K$  rather than general simplex. For some splitting  $\Delta$  of  $K$ , we define

$$S_k^1(\Delta) = \{s \in C^1(K) : s|_{\tau} \in P_k(\tau), \tau \in \Delta\} \quad (2.12)$$

to be the space of continuously differentiable piecewise polynomials of degree  $d$ . When  $k = 2$  and  $\Delta \in \{\Delta_{PS6}(T), \Delta_{PS12}(T)\}$ , we obtain the spaces for the quadratic Powell-Sabin splines in Figs. 1c and 1d. When  $k = 3$  and  $\Delta = \Delta_A(K)$ , this is the standard HCT space.

Letting  $\mathcal{E}$  denote the edges of  $K$ , we also obtain the reduced space

$$\tilde{S}_3^1(\Delta) = \{s \in S_3^1(\Delta) : \frac{\partial s}{\partial \mathbf{s}}|_e \in P_1(e), e \in \mathcal{E}\}. \quad (2.13)$$

Recently, Groselj and Knez [Groselj and Knez 2022] have constructed a generalization of the space  $S_k^1(\Delta)$  to higher-order polynomials while retaining  $C^1$  continuity and full approximating power. They define the supersmooth space

$$S_k(\Delta_A(K)) = S_k^1(\Delta_A(K)) \cap C^{d-1}(\mathbf{v}_0), \quad (2.14)$$

where  $\mathbf{v}_0$  denotes the interior point of the Alfeld split  $\Delta_A(K)$ . This space has greater than  $C^1$  continuity within the triangle  $K$ , although it only joins across triangles with  $C^1$  continuity.

Now, we can define the degrees of freedom used to parametrize the splines over Powell-Sabin and Alfeld splits. It is well known that the quadratic space  $S_2^1(\Delta_{PS6}(K))$  is nine-dimensional. The degrees of freedom are shown in Fig. 3a, and can be taken to be:

- $\delta_v$  for each vertex  $v$  of  $K$ ,
- $\delta_v^s$  for each vertex  $v$  of  $K$  and for  $s$  each Cartesian direction  $x$  and  $y$ .

Over the 12-way split, we have  $\dim S_2^1(\Delta_{PS12}(K)) = 12$ . The degrees of freedom are shown in Fig. 3b, and can be taken to be:

- $\delta_v$  for each vertex  $v$  of  $K$ ,
- $\delta_v^s$  for each vertex  $v$  of  $K$  and for  $s$  each Cartesian direction  $x$  and  $y$ .
- $\mu_e^{\mathbf{n}_e}$  for each edge  $e$  of  $K$ , where  $\mathbf{n}_e$  is the normal to each edge.

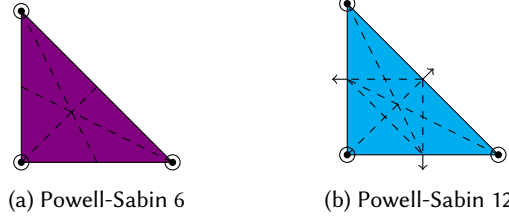


Fig. 3. Quadratic  $C^1$  macroelements on Powell-Sabin splits. Hollow circles represent derivative evaluation for each Cartesian direction, the arrows represent normal derivative moments along edges.

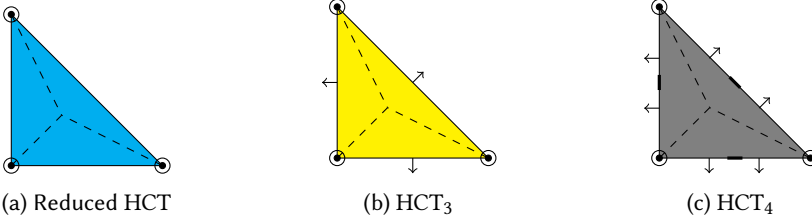


Fig. 4. HCT-type  $C^1$  macroelements on the Alfeld split. Solid lines represent moments along edges.

The HCT space,  $S_3^1(\Delta_A(K))$ , is also 12-dimensional, and we may take the degrees of freedom to be the same as for  $S_2^1(\Delta_{PS12}(K))$ . (While these are mathematically the same, we note that a numerical implementation must respect that fact that the Powell-Sabin split divides the edges of  $K$  and hence a composite quadrature rule must be used). The reduced HCT space  $\tilde{S}_3(\Delta_A(K))$  has only dimension 9, and one can take the same vertex value and derivative degrees of freedom as for  $S_2^1(\Delta_{PS6}(K))$ .

The higher-order HCT spaces require additional edge and interior degrees of freedom. For  $S_k(\Delta_A(K))$ , we take degrees of freedom

- $\delta_v$  for each vertex  $v$  of  $K$ ,
- $\delta_v^s$  for each vertex  $v$  of  $K$  and for  $s$  each Cartesian direction  $x$  and  $y$ .
- $\mu_{e,q^1}^{\mathbf{n}}$  for each edge  $e$  of  $K$  and  $q^1$  in a basis for  $P_{k-3}(\mathbf{e})$ . Here,  $\mathbf{n}$  is the normal to edge  $e$
- If  $k > 3$ , take the additional moments:
  - $\mu_{e,q^2}$ , for each edge  $e$  of  $K$  and  $q^2$  in a basis for  $P_{k-4}(\mathbf{e})$ .
  - $\mu_{K,q^3}$  for each  $q^3$  in a basis for  $P_{k-4}(K)$ .

Although any choice of polynomial bases will suffice for edge and interior moments, we have made some specific choices that expedite the mapping from a reference element and also, incidentally, give a hierarchical basis. It is important for deriving the transformations that the normal

derivative moments and moments of the trace are taken against complementary functions. In particular,  $q_2$  should be taken as the derivative of the polynomials in  $q_1$ . We take the polynomials  $q^1$  on the edge  $e$  to be the Jacobi polynomials  $P_i^{(1,1)}$  for  $0 \leq i \leq k-3$  mapped to that edge. Then,  $q^2$  are the derivatives of the Jacobi polynomials  $\frac{d}{ds} P_i^{(1,1)}(s)$  for  $1 \leq i \leq k-3$ . Finally, we take the polynomials  $q^3$  on a triangle to be the Dubiner polynomials of degree  $k-4$ , ordered hierarchically so that all polynomials of one degree occur before any of the next higher degree.

## 2.5 Stokes elements

The Stokes equations model creeping flow of an incompressible viscous fluid, and are a widely-studied model from both physical and numerical perspectives. The spaces in which they are discretized must be chosen in tandem to satisfy the inf-sup condition, and construction of stable discretization of this system has driven much research in finite elements. Finding pairs of spaces for which the discrete velocity is divergence free *pointwise* rather than in some weak sense is a particular challenge, especially on simplicial meshes. Scott and Vogelius [Brenner and Scott 2008; Scott and Vogelius 1984] show that, up to certain mesh restrictions, one may use continuous velocities of degree  $k$  and discontinuous pressures of degree  $k-1$ . Generally, this requires  $k \geq 4$  on triangles and  $k \geq 6$  on tetrahedra, but one may take  $k \geq 2$  for triangles and  $k \geq 3$  for tetrahedra provided that the mesh is obtained by barycentric refinement of an existing simplicial mesh. Even with the refined mesh, this is a major decrease in cost compared to high degree polynomials. For example, each quartic velocity component requires 15 degrees of freedom per triangle, while quadratics on the split mesh require only 10, as shown in Fig. 2b.

Other pairs with macroelements can give pointwise divergence-free velocities with continuous pressures, which allows smaller approximating spaces. These lie in a differential complex and also ensure the divergence-free condition holds pointwise, but this work seems to be the first realization of them in practice. In particular, we consider the Guzmán–Neilan and Alfeld–Sorokina macroelements.

It is possible to obtain a minimal inf-sup stable Stokes pair that includes the linears on the unsplit cell, plus some face bubbles. The motivation behind enriching with face bubbles is to control the divergence by adding normal degrees of freedom on each face. A non-macroelement example is the Bernardi–Raugel element, which is defined by enriching linear vector fields with normal face bubbles [Bernardi and Raugel 1985]. It achieves inf-sup stability when paired with piecewise constants. Nevertheless, the face bubbles are of degree  $d$ , and their divergence is of degree  $d-1$ , so the divergence-free constraint can only be weakly enforced when testing against piecewise constants. That is, the integral of the divergence over each cell vanishes in this case.

In two dimensions, Arnold and Qin [Arnold and Qin 1992] proposed a macroelement on the Alfeld split with divergence-free quadratic face bubbles. This element pairs with piecewise constants on the unsplit mesh, and may be regarded as a modification of Bernardi–Raugel. Here, the face bubbles are modified by subtracting a piecewise polynomial on the split cell that also vanishes on the boundary, matching the divergence of the Bernardi–Raugel face bubble. More recently, this construction has been extended to any dimension by Guzmán and Neilan [Guzmán and Neilan 2018]. Fig. 5a shows the degrees of freedom of this element on the triangle.

Macroelements also enable divergence-free formulations for Stokes with continuous pressure elements. These are naturally posed in  $H^1(\text{div}) \times H^1$ , where  $H^1(\text{div}) = \{v \in H^1 : \text{div } v \in H^1\}$ . The quadratic Alfeld–Sorokina macroelement [Alfeld and Sorokina 2016] is constructed as the piecewise quadratics on an Alfeld split with  $C^0$  divergence. This construction works in any dimension, but is only inf-sup stable in 2D. It is also shown in [Guzmán and Neilan 2018] that an inf-sup stable Stokes element with  $C^0$  divergence can be obtained in three dimensions by enriching the Alfeld–Sorokina

quadratic macroelement with the same cubic divergence-free face bubbles. Fig. 5b shows the degrees of freedom for this element in two dimensions, which are those of unsplit quadratic vectors plus the divergence at each vertex.

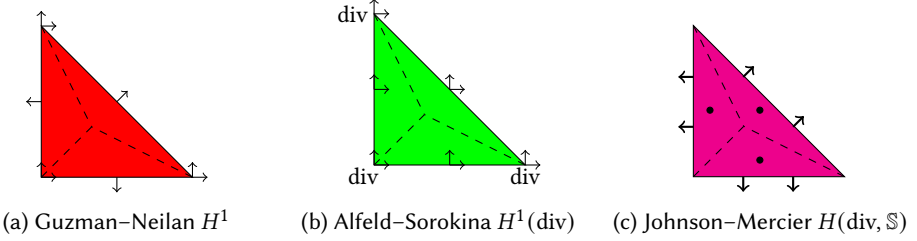


Fig. 5. Lowest-order macroelements for the Stokes and elasticity complexes. The thin arrows in Guzman–Neilan and Alfeld–Sorokina represent evaluation of vector components. The thicker arrows in Johnson–Mercier represent moments of the normal-normal and normal-tangential components of a tensor.

## 2.6 The Johnson–Mercier element

The elements of Johnson and Mercier [Johnson and Mercier 1978] provide symmetric  $H(\text{div})$ -conforming tensors suitable for the discretization of the Hellinger–Reissner formulation of elasticity or stress-velocity formulations of incompressible flow. Recently, a general formulation for simplicial elements in  $\mathbb{R}^d$  has been given for all  $d \geq 2$  [Gopalakrishnan et al. 2024]. Letting  $\mathbb{S}^d$  denote the space of symmetric  $d \times d$  tensors, they discretize  $H(\text{div}; \mathbb{S}^d)$ .

Let  $K$  be a simplex in  $\mathbb{R}^d$ , split into  $d + 1$  subcells via the Alfeld split. We let  $\Sigma_h(K)$  denote the div-conforming space of all functions mapping  $K$  into  $\mathbb{S}^d$ :

$$\Sigma_h(K) = \{ \tau \in H(\text{div}, K, \mathbb{S}^d) : \tau|_{K_i} \in P_1(K_i, \mathbb{S}^d), 1 \leq i \leq d + 1 \},$$

where  $P_1(K_i, \mathbb{S}^d)$  just comprises symmetric tensor-valued functions whose components are all linear polynomials over subcell  $K_i$ .

This space has dimension  $(d + \frac{1}{2})d(d + 1)$ , which is 15 for triangles and 42 for tetrahedra and hence much smaller than the Arnold–Winther elements. Fig. 5c shows the Johnson–Mercier element on a triangle. Degrees of freedom parametrizing space come in two kinds:

- For each facet of codimension 1,  $f$ , with unit normal  $\mathbf{n}$ , the integral moments of each component of  $\tau \mathbf{n}$  against all linear polynomials over  $f$ .
- The integral average of each independent component of  $\tau$  over  $K$ .

## 3 CODE DEVELOPMENT

Here, we describe the development within FIAT itself necessary to enable reference element construction of macroelements, and the development through other packages to enable full integration within Firedrake.

### 3.1 FIAT development

The first major development within FIAT is the introduction of a `SimplicialComplex` class. This extends the existing classes modeling reference simplices by allowing multiple subcells. The simplicial complex defines the local topology and connectivity of the subcells and also provides rules to geometric information such as normal and tangent vectors to the facets in the complex. Derived from this class is a `SplitSimplicialComplex` whose subclasses encode particular splittings



of an existing simplicial complex. The constructor for this class simply requires the parent complex to be split, and a list of the locations of vertices and topology of the new complex. From this, essential parent-to-child relationships, such as which parent facets of the original cell contain which facets of the splitting, are programmatically constructed.

FIAT already provides a wide suite of general quadrature rules. In [Brubeck et al. 2024], we described the inclusion of the Xiao–Gimbutas rules [Xiao and Gimbutas 2010]. We now provide a `MacroQuadrature` class that tiles a given simplicial quadrature rule over each subcell or facet in simplicial complex to give an appropriate composite quadrature rule. When finite element methods employ elements over different splittings, one requires quadrature rules accurate on both complexes. To support this, simplicial complexes also provide a kind of comparison operator indicating when one complex is a refinement of another.

FIAT builds nodal basis functions as linear combinations of an *expansion set* – typically some set of orthonormal polynomials – and this theme is maintained with macroelements. We have the standard  $L^2$  orthogonal polynomials [Karniadakis and Sherwin 2005], computed using the singularity-free recurrences in [Kirby 2010]. These polynomials can be tiled without continuity across the complex, and we have also implemented the modified  $C^0$  expansion set described in [Karniadakis and Sherwin 2005]. Additionally, we can construct bases for spaces with higher continuity by finding the null space of a collection of functionals defining jumps across boundaries in a cell complex.

FIAT constructs the nodal basis for a finite element – including macroelements – by pairing a basis for the approximating space with a list of degrees of freedom containing a basis for the dual space, as described in prior work [Kirby 2004]. This key aspect of FIAT has required no further internal modification, but care must be taken that functionals defining integral moments over a split complex use an appropriate composite quadrature rule.

Lagrange finite elements over macro cells may be constructed in one of two ways. First, the user may instantiate the Lagrange finite element over a `SplitSimplicialComplex`, in which case a suitable expansion set is chosen. Alternatively, one may provide an unsplit simplex and the optional `variant` keyword. When this keyword provides a splitting such as `'iso'` or `'alfeld'`, the reference simplex is appropriately split.

### 3.2 FInAT development

FInAT [Homolya et al. 2017] provides the main basis function interface to the rest of Firedrake. While it can provide abstract syntax for evaluating and manipulating basis function evaluation, enabling optimizations such as sum-factorization, it also provides many other services. We are not fully using these features with macroelements, but FInAT also plays a critical role in enabling the non-standard transformations used when finite elements use derivative degrees of freedom [Kirby and Mitchell 2019]. This feature is critical to enabling the many of the macroelements we have enabled, and some of the basis transformations are described below.

### 3.3 TSFC development

Firedrake uses `tsfc` [Homolya et al. 2018] to generate code for evaluating variational forms. Our macroelement implementation has required only minor changes within `tsfc`. In particular, the algorithm for quadrature selection had to be generalized to select a composite rule suitable for all functions (including those defined over splittings) appearing in a given integral in the form.

Macroelements present an opportunity for future optimizations within the form compiler. Currently, `tsfc` uses a “flattened” quadrature rule and table of basis values. Alternatively, each basis function can be assembled from some shape functions defined over the subcells. Utilizing this substructure could give a minor speedup for low-order elements. High-continuity elements on

simple splits have relatively limited sparsity and so likewise might obtain limited benefit. On the other hand,  $C^0$  elements defined over higher-order iso-type splits would stand to gain from iterating over subelements, but we have focused on feature inclusion rather than the potentially invasive modifications to optimize this case.

### 3.4 Firedrake development

Somewhat suprisingly, our design of macroelements in FIAT and its interfaces with FInAT and tsfc are rather self-contained and spawned no internal Firedrake development. One simply obtains a macroelement space by providing the element name to the FunctionSpace constructor. To obtain Lagrange-type macroelements, one provides the variant keyword. For example:

```
V0 = FunctionSpace(mesh, 'HCT', 3)
V1 = FunctionSpace(mesh, 'Lagrange', 2, variant='alfeld')
```

In fact, the systematic modifications in the supporting packages meant that the Firedrake pull request only added tests of accuracy with macroelements.

## 4 TRANSFORMATION THEORY

When basis functions are constructed on some reference domain  $\hat{K}$ , they must be mapped somehow to each cell  $K$  in the given mesh. Classically, a mapping  $F : K \rightarrow \hat{K}$  (affine for straight-sided simplices) is constructed per Fig. 6, and one obtains a pullback in the standard way. For each  $\hat{f} : \hat{K} \rightarrow \mathbb{R}$ , define  $F^*(\hat{f}) \equiv f : K \rightarrow \mathbb{R}$  by

$$f = F^*(\hat{f}) = \hat{f} \circ F, \quad (4.1)$$

and we also have the push-forward of a functional  $n$  acting on functions over  $K$  to those over  $\hat{K}$  by

$$F_*(n) = n \circ F^*. \quad (4.2)$$

For Lagrange elements, the pullback maps the reference element basis functions exactly to the physical element basis functions, and the push-forward maps point evaluation on  $K$  to point evaluation on the point's preimage points under  $F$ . However,  $C^1$  and many other finite elements utilize derivatives and other degrees of freedom that are not preserved under push-forward, as shown in Fig. 7, and this complicates the usage of a reference element. Similar issues are observed for  $H(\text{div})$  finite elements and the contravariant Piola map – certain elements like Raviart–Thomas and Brezzi–Douglas–Marini are mapped perfectly under the Piola pull-back, while most other elements are not. Here, we apply the theory developed in [Aznaran et al. 2022; Kirby 2018] to some of our newly-enabled macroelements. The goal of this theory is to identify a matrix  $M$  such that the vector of basis functions over  $K$  can be constructed by  $M$  times the vector of pullbacks of reference element basis functions. It is often the case that the transpose of this matrix, which relates the push-forwards of physical nodes to the reference element nodes, is easier to construct mathematically. At any rate, this matrix is typically quite sparse and so forming it is much cheaper than directly building the basis functions on each cell.

### 4.1 HCT

The HCT triangle provides a  $C^1$ -conforming element with 12 degrees of freedom and piecewise cubic polynomials. We divide any triangle  $T$  into three sub-triangles  $T_1, T_2, T_3$  by connecting each vertex of  $T$  to the barycenter. The function space  $P^{HCT}(T)$  then consists of cubic polynomials over each  $T_i$  that are  $C^1$  across internal edges. This space is known to be twelve-dimensional, and is parameterized by function values and gradients at the vertices together with normal derivatives on each edge.

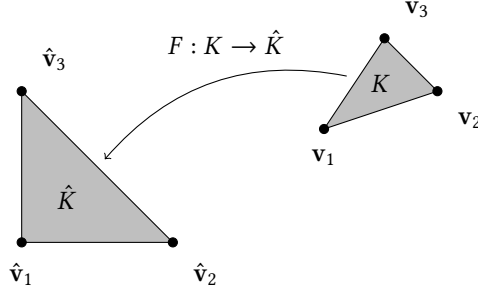


Fig. 6. Affine mapping to a reference cell  $\hat{K}$  from a typical cell  $K$ . Note that here  $F$  maps from the physical cell  $K$  to the reference cell  $\hat{K}$  rather than the other way around.

We can write the nodes for HCT in a vector as

$$\mathcal{N} = [\delta_{v_1} \quad \nabla_{v_1}^\top \quad \delta_{v_2} \quad \nabla_{v_2}^\top \quad \delta_{v_3} \quad \nabla_{v_3}^\top \quad \mu_{e_1}^{n_1} \quad \mu_{e_2}^{n_2} \quad \mu_{e_3}^{n_3}]^\top. \quad (4.3)$$

For the reference element, we define the edge nodes to use integral averages rather than moments:

$$\hat{\mu}_{\hat{e}}^s(f) = \frac{1}{|\hat{e}|} \int_{\hat{e}} \hat{s} \cdot \hat{\nabla} f \, d\hat{s}. \quad (4.4)$$

Then, we enumerate the reference element nodes as

$$\hat{\mathcal{N}} = [\delta_{\hat{v}_1} \quad \hat{\nabla}_{\hat{v}_1}^\top \quad \delta_{\hat{v}_2} \quad \hat{\nabla}_{\hat{v}_2}^\top \quad \delta_{\hat{v}_3} \quad \hat{\nabla}_{\hat{v}_3}^\top \quad \hat{\mu}_{\hat{e}_1}^{\hat{n}_1} \quad \hat{\mu}_{\hat{e}_2}^{\hat{n}_2} \quad \hat{\mu}_{\hat{e}_3}^{\hat{n}_3}]^\top. \quad (4.5)$$

This redefinition eliminates the need for logic indicating to which reference element edges the edges of each triangle correspond in the typical case of a right isosceles reference triangle.

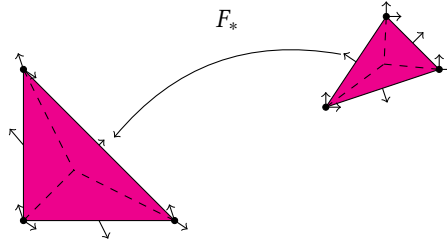


Fig. 7. Pushing forward the HCT derivative nodes in physical space does *not* produce the reference derivative nodes.

Now, the major issue in transforming the HCT element is that the push-forward of the physical nodes does not align with the reference nodes. The transformation theory proceeds by constructing a *completion* of the set of nodes in the reference and physical spaces. These are constructed so that the span of the push-forwards of the physical node completion coincides with the span of the reference completion. To do this, we first introduce  $\mu_e^t(f)$  per (2.10) to be the integral moment of the tangential derivative along edge  $e$  of the triangle. To find the nodal completion for the reference dual, we take  $\hat{\mu}_e^t$  to be the integral average of the tangential derivative along a reference edge. We define

$$\mathcal{M}_i = [\mu_{e_i}^{n_i} \quad \mu_{e_i}^{t_i}]^\top \quad (4.6)$$

to be the vector of the moments of the normal and tangential derivatives on a particular edge. We also let  $\widehat{\mathcal{M}}_i$  contain the corresponding reference element nodes.

Then, the compatible nodal completion for the HCT element is

$$\mathcal{N}^c = [\delta_{\mathbf{v}_1} \quad \nabla_{\mathbf{v}_1}^\top \quad \delta_{\mathbf{v}_2} \quad \nabla_{\mathbf{v}_2}^\top \quad \delta_{\mathbf{v}_3} \quad \nabla_{\mathbf{v}_3}^\top \quad \mathcal{M}_1^\top \quad \mathcal{M}_2^\top \quad \mathcal{M}_3^\top]^\top. \quad (4.7)$$

Then, we enumerate the completed reference element nodes as

$$\widehat{\mathcal{N}}^c = [\delta_{\hat{\mathbf{v}}_1} \quad \widehat{\nabla}_{\hat{\mathbf{v}}_1}^\top \quad \delta_{\hat{\mathbf{v}}_2} \quad \widehat{\nabla}_{\hat{\mathbf{v}}_2}^\top \quad \delta_{\hat{\mathbf{v}}_3} \quad \widehat{\nabla}_{\hat{\mathbf{v}}_3}^\top \quad \widehat{\mathcal{M}}_1^\top \quad \widehat{\mathcal{M}}_2^\top \quad \widehat{\mathcal{M}}_3^\top]^\top. \quad (4.8)$$

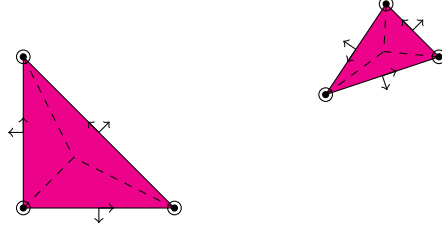


Fig. 8. Nodal sets  $\widehat{\mathcal{N}}^c$  and  $\mathcal{N}^c$  giving the compatible nodal completion of  $N$  and  $\widehat{N}$  for an HCT element and reference element are formed by including tangential derivatives along with normal derivatives at each edge midpoint.

To apply the general pullback theory, we write the transformation as

$$M^\top = V = EV^cD, \quad (4.9)$$

where  $D \in \mathbb{R}^{15 \times 12}$  expresses the completed nodes in terms of the given physical nodes, mapping  $N$  to  $\mathcal{N}^c$ .  $V^c \in \mathbb{R}^{15 \times 15}$  is a block diagonal matrix relating the push-forward of the reference nodal completion to the physical nodal completion, and  $E \in \mathbb{R}^{12 \times 15}$  is a Boolean matrix selecting actual finite element nodes from the completion.

Here,  $D$  follows quite naturally. Clearly, the rows corresponding to members of  $\mathcal{N}^c$  also appearing in  $N$  will just have a single nonzero in the appropriate column. The nodes in  $\mathcal{N}^c$  not in  $N$  are just integrals of quantities over edges, and we can use the Fundamental Theorem of Calculus to perform this task. Let  $\mathbf{e}$  be an edge running from vertex  $\mathbf{v}_a$  to  $\mathbf{v}_b$  with unit tangent  $\mathbf{t}$ . We have

$$\mu_{\mathbf{e}}^{\mathbf{t}}(f) = \int_{\mathbf{e}} \mathbf{t} \cdot \nabla f \, ds = f(\mathbf{v}_b) - f(\mathbf{v}_a) = \delta_{\mathbf{v}_b}(f) - \delta_{\mathbf{v}_a}(f) \quad (4.10)$$

Putting this together with the node orderings in (4.7) and (4.3), we write  $D$  as a block matrix segregating the vertex and edge nodes with

$$D = \left[ \begin{array}{c|c} I & 0 \\ \hline D_{12} & D_{22} \end{array} \right]. \quad (4.11)$$

Here,  $I$  is the  $9 \times 9$  identity matrix, and

$$D_{12} = \begin{bmatrix} 0 & 0 & 0 & 0 & 0 & 0 & 0 & 0 & 0 \\ 0 & 0 & 0 & -1 & 0 & 0 & 1 & 0 & 0 \\ 0 & 0 & 0 & 0 & 0 & 0 & 0 & 0 & 0 \\ -1 & 0 & 0 & 1 & 0 & 0 & 0 & 0 & 0 \\ 0 & 0 & 0 & 0 & 0 & 0 & 0 & 0 & 0 \\ -1 & 0 & 0 & 0 & 0 & 0 & 1 & 0 & 0 \end{bmatrix}, \quad D_{22} = \begin{bmatrix} 1 & 0 & 0 \\ 0 & 0 & 0 \\ 0 & 1 & 0 \\ 0 & 0 & 0 \\ 0 & 0 & 1 \\ 0 & 0 & 0 \end{bmatrix}. \quad (4.12)$$

Then,  $V^c$  is obtained by relating the push-forwards of  $\mathcal{N}^c$  to  $\widehat{\mathcal{N}}^c$ . The vertex degrees of freedom transform just as those for the Hermite triangle [Kirby 2018] and lead to blocks with 1 and the cell Jacobian. To transform the edge degrees of freedom, we note that  $\mu_e^n$  and  $\mu_e^t$  together comprise the moments of the gradient along edge  $e$  in an orthogonal coordinate system. Given the orthogonal unit vectors  $\mathbf{n}$  and  $\mathbf{t}$ , we can define an orthogonal matrix  $G$  by:

$$G = [\mathbf{n} \quad \mathbf{t}]^\top. \quad (4.13)$$

In particular,  $G_i$  to have the normal and tangential vectors to edge  $i$  of triangle  $K$  in its columns and  $\widehat{G}_i$  those for triangle  $\widehat{K}$ . By changing the gradient to normal/tangential coordinates:

$$\nabla_x = G^\top \nabla_x^{\text{nt}}. \quad (4.14)$$

Now, we can connect physical and reference gradients in the normal/tangential coordinate system via the chain rule

$$\nabla_x^{\text{nt}} = G J^\top \widehat{G}^\top \widehat{\nabla}_{\widehat{\mathbf{x}}}^{\text{nt}}. \quad (4.15)$$

Now, for any vector  $\mathbf{s}$ , edge  $\mathbf{e}$ , and smooth function  $f = f \circ F$ , we have

$$\int_{\mathbf{e}} \mathbf{s} \cdot \nabla f \, ds = \int_{\widehat{\mathbf{e}}} \mathbf{s} \cdot \widehat{\nabla} f \circ F \, ds = \int_{\widehat{\mathbf{e}}} \mathbf{s} \cdot \widehat{\nabla} f J_{\mathbf{e}, \widehat{\mathbf{e}}} d\widehat{s}, \quad (4.16)$$

where the Jacobian  $J_{\mathbf{e}, \widehat{\mathbf{e}}}$  is just the ratio of the length of  $\mathbf{e}$  to that of the corresponding reference element edge  $\widehat{\mathbf{e}}$ . Applying this to the normal and tangential moments and using (4.15), we have that:

$$\mathcal{M}_i = |\mathbf{e}_i| G_i J^\top \widehat{G}_i^\top \widehat{\mathcal{M}}_i, \quad (4.17)$$

where the factor of  $|\widehat{\mathbf{e}}_i|$  in the denominator of the Jacobian is merged with the reference element moments to produce  $\widehat{\mathcal{M}}_i$ . Hence, the slight modification of reference element nodes avoids extra data structures or logic in identifying reference element edge numbers.

We identify the matrices

$$B_i = \widehat{G}_i^\top J^{-\top} G / |\mathbf{e}_i|. \quad (4.18)$$

Then, we can also write  $V^c$  in a block diagonal form

$$V^c = \left[ \begin{array}{c|c} V_v^c & 0 \\ \hline 0 & V_e^c \end{array} \right], \quad (4.19)$$

where  $V_v^c$  is itself a block  $3 \times 3$  matrix with three copies of the  $3 \times 3$  matrix

$$\begin{bmatrix} 1 & 0 \\ 0 & J^{-T} \end{bmatrix} \quad (4.20)$$

along the diagonal.  $V_e^c$  is also a block  $3 \times 3$  matrix

$$V_e^c = \begin{bmatrix} B_1 & 0 & 0 \\ 0 & B_2 & 0 \\ 0 & 0 & B_3 \end{bmatrix}. \quad (4.21)$$

The Boolean extraction matrix  $E \in \mathbb{R}^{12 \times 15}$  simply takes entries of  $\widehat{N}$  from  $\widehat{\mathcal{N}}^c$ , so that

$$E_{ij} = \begin{cases} 1, & i = j \text{ and } 1 \leq i \leq 9 \text{ or } i, j \in \{(10, 10), (11, 12), (12, 14)\}, \\ 0, & \text{otherwise.} \end{cases}$$

The reduced HCT element requires a similar but more complicated approach. For this element, the function space is not preserved under affine mapping. We have adapted the techniques developed for the Bell element in [Kirby 2018] to handle this case.

## 4.2 High-order HCT

We briefly describe the generalization of HCT to high order, using a similar space as the one from [Grošelj and Knez 2022]. In an effort to reduce the number of interior degrees of freedom while maintaining the same order of accuracy as the minimally  $C^1$  polynomials of degree  $k \geq 3$ , they enforce  $C^{k-1}$  supersmoothness at the interior vertex of the split, which is chosen as the incentor to allow for positive basis functions defined in terms of Bernstein–Bézier polynomials. To enable a reference element approach, we instead construct the supersmooth  $C^1$  subspace by constraining the  $C^0$  hierarchical basis on an Alfeld split using the barycenter, which does not yield positive basis functions.

The high-order HCT nodes are an augmentation of (4.3). The vertex-based degrees of freedom remain unchanged, i.e., we keep point evaluation and the gradient at each exterior vertex.

The edge-based degrees of freedom come in two kinds. The first kind are normal derivative moments against Jacobi polynomials  $P_i^{(1,1)}$ ,

$$\hat{\mu}_{\mathbf{e},i}^n(f) = \frac{1}{|\mathbf{e}|} \int_{\mathbf{e}} P_i^{(1,1)}(\hat{s}) \mathbf{n} \cdot \nabla f \, ds, \quad i = 0, \dots, k-3. \quad (4.22)$$

Here, we introduce the normalized variable  $\hat{s} \in [-1, 1]$ , defined in terms of the length  $s$  along  $\mathbf{e}$  as  $\hat{s} = 2(s/|\mathbf{e}|) - 1$ . We have slightly altered the notation, using the second subscript to index into a set of polynomials rather than as a polynomial itself. The second kind are trace moments against the derivative of Jacobi polynomials

$$\mu_{\mathbf{e},i}(f) = \int_{\mathbf{e}} \frac{d}{ds} P_i^{(1,1)}(\hat{s}) f \, ds, \quad i = 1, \dots, k-3. \quad (4.23)$$

For  $k \geq 4$ , the interior degrees of freedom are integral moments against a basis  $\{q_i\}$  for  $P_{k-4}(K)$ ,

$$\mu_{K,i}(f) = \int_K q_i f \, dx. \quad (4.24)$$

For the edge degrees of freedom, the Jacobi weights  $(1, 1)$  have been chosen to produce hierarchical edge-based basis functions. Using the orthogonality property

$$\int_{-1}^1 (\hat{s} + 1)^\alpha (\hat{s} - 1)^\beta P_i^{(\alpha,\beta)}(\hat{s}) P_j^{(\alpha,\beta)}(\hat{s}) \, d\hat{s} = c_i^{(\alpha,\beta)} \delta_{ij}, \quad (4.25)$$

the identity  $\frac{d}{d\hat{s}} P_i^{(\alpha,\beta)}(\hat{s}) = d_i^{(\alpha,\beta)} P_{i-1}^{(\alpha+1,\beta+1)}(\hat{s})$ , and the enforcement of vanishing value and tangential derivative at the vertices, we deduce that the edge-based basis functions associated with  $\mu_{\mathbf{e},i}$  have a trace proportional to  $(\hat{s} + 1)^2 (\hat{s} - 1)^2 P_{i-1}^{(2,2)}(\hat{s})$ . Similarly, basis functions associated with  $\mu_{\mathbf{e},i}^n$  have normal derivative trace proportional to  $(\hat{s} + 1)(\hat{s} - 1) P_i^{(1,1)}(\hat{s})$ .

On each edge  $\mathbf{e}$ , for a fixed value of  $i > 0$ , to find the nodal completion of the normal derivative moments  $\mu_{\mathbf{e},i}^n$ , again we take the tangential derivative moments  $\mu_{\mathbf{e},i}^t$ . These can conveniently be computed from the trace moments  $\mu_{\mathbf{e},i}$  and the value of  $f$  at the endpoints  $\mathbf{v}_a, \mathbf{v}_b$  of  $\mathbf{e}$ , by integrating by parts and exploiting the fact that the trace moments are defined against  $\frac{d}{ds} P_i^{(1,1)}$ ,

$$\mu_{\mathbf{e},i}^t(f) = \int_{\mathbf{e}} P_i^{(1,1)}(\hat{s}) \mathbf{t} \cdot \nabla f \, ds = -\mu_{\mathbf{e},i}(f) + P_i^{(1,1)}(1) \delta_{\mathbf{v}_b}(f) - P_i^{(1,1)}(-1) \delta_{\mathbf{v}_a}(f). \quad (4.26)$$

Note that (4.10) still holds for  $i = 0$ . The transformation of  $\mu_{\mathbf{e},i}^n$  then carries out in a very similar fashion, except that there is additional coupling with  $\mu_{\mathbf{e},i}$ .

We may also extend this construction to Argyris elements of arbitrarily high order. The only difference is that the Jacobi weights need to be chosen as  $(2, 2)$ , due to the presence of second derivative degrees of freedom at vertices.

## 5 NUMERICAL EXAMPLES

Our computations were performed with Firedrake installed on a Linux workstation with an AMD Ryzen Threadripper PRO 3995WXs CPU with 64 cores, 128 threads, a clock-rate of 4.2 GHz, and 256 GiB of RAM.

### 5.1 Stokes flow

Here, we consider two formulations of the Stokes equations of incompressible flow for which our macroelement technology provides effective discretization. First, we consider the standard pressure-velocity formulation, written in weak form as

$$\begin{aligned} (2\nu\boldsymbol{\varepsilon}(\mathbf{u}), \boldsymbol{\varepsilon}(\mathbf{v})) - (p, \operatorname{div} \mathbf{v}) &= (\mathbf{f}, \mathbf{v}), \\ -(\operatorname{div} \mathbf{u}, q) &= 0. \end{aligned} \quad (5.1)$$

Here,  $\mathbf{u}$  and  $p$  represent the fluid velocity and pressure in some domain  $\Omega$  in two or three spatial dimensions. The parameter  $\nu$  is known as the kinematic viscosity, and the system may be driven by body forces  $\mathbf{f}$  (e.g. gravity), and boundary conditions on the velocity and/or stress  $\boldsymbol{\sigma} := 2\nu\boldsymbol{\varepsilon}(\mathbf{u}) - pI$  must be included to close to system.

The Stokes equations may also be formulated in terms of the stress  $\boldsymbol{\sigma}$  itself and velocity  $\mathbf{u}$ , which may be of interest in non-Newtonian flows.

$$\begin{aligned} \frac{1}{2\nu} (\boldsymbol{\sigma}, \boldsymbol{\tau}) - \frac{1}{2d\nu} (\operatorname{tr} \boldsymbol{\sigma}, \operatorname{tr} \boldsymbol{\tau}) + (\mathbf{u}, \operatorname{div} \boldsymbol{\tau}) &= 0, \\ (\operatorname{div} \boldsymbol{\sigma}, \mathbf{v}) &= (\mathbf{f}, \mathbf{v}). \end{aligned} \quad (5.2)$$

Three-field formulations that include pressure are also possible.

Formulations that include symmetric stress tensor require special treatment. One may use the Arnold–Winther elements as in [Carstensen et al. 2012], or weakly enforce the symmetry of the stress tensor [Gopalakrishnan et al. 2020]. The Johnson–Mercier element provides a conforming and symmetric stress approximation via a low-cost macroelement with only piecewise linear polynomials.

Here, we attempt to assess the accuracy and cost of various methods for both the velocity-pressure and stress-velocity forms of the Stokes equations in two and three dimensions. We use the method of manufactured solutions, selecting the right-hand side and boundary data such that the true solution to the equations is some known smooth function. We force both forms of the equation (velocity-pressure and stress-velocity) to yield the same pressure, velocity, and stress.

Then, we partition the unit square into an  $N \times N$  mesh of squares, subdividing each into two right triangles. The unit cube is partitioned into an  $N \times N \times N$  mesh of cubes, with each subdivided into six tetrahedra. We approximate (5.1) with several finite element families on each mesh. We use the standard  $P_2 - P_1$  Taylor–Hood and the  $P_2^{\text{iso}} - P_1$  elements to provide a point of comparison to classical elements. We also use Scott–Vogelius macroelements with continuous  $P_d$  velocity and discontinuous  $P_{d-1}$  pressures on the Alfeld split, the Alfeld–Sorokina velocity element paired with  $C^0P_1$  velocity on the Alfeld split and the Guzman–Nelán element paired with piecewise constants. Finally, we approximate (5.2) using the Johnson–Mercier macroelement paired with discontinuous linear velocities.

To measure the enforcement of incompressibility constraint  $\operatorname{div} \mathbf{u} = 0$ , we compute the functional

$$\left( \sum_K \|\operatorname{div} \mathbf{u}\|_K^2 + \sum_e \frac{1}{h_e} \|[\![ \mathbf{u} \cdot \mathbf{n} ]\!] \|_e^2 \right)^{1/2}, \quad (5.3)$$

where  $\|\cdot\|_K$  denotes the  $L^2$  norm over a cell and  $\|\cdot\|_e$  the  $L^2$  norm over an edge. The velocity-pressure formulation gives an  $H^1$ -conforming discretization, so this quantity simplifies to the  $L^2$  norm of the divergence.

Fig. 9 shows the error in the velocity, pressure, stress, and divergence versus the number of vertices in an  $N \times N$  mesh of squares, each subdivided into two triangles. In the velocity/pressure formulation, we solve the system and then compute a stress approximation via  $\sigma = \epsilon(u) - pI$ , and we similarly postprocess the stress to find the pressure in the stress-velocity formulation. For both formulations we set  $\nu = 1$ , and the theoretically predicted rates of convergence are observed. Taylor–Hood method actually gives the best velocity and stress approximations on a given mesh, followed by the Alfeld–Sorokina method, with these two also giving the best approximation of the pressure. The Guzman–Neilan approach uses a lower-order pressure approximation, which limits the overall accuracy of the method. The Taylor–Hood, iso, and Johnson–Mercier methods have quite a large residual divergence, while the other three approaches enforce the divergence-free condition to high accuracy. We may summarize these results by saying that Taylor–Hood may be preferred if a pointwise divergence-free condition is not critical, while Alfeld–Sorokina may be preferred if it is. The Johnson–Mercier approach is competitive and may be of interest for more complex rheology.

Fig. 10 shows analogous results for three dimensions. Here, we note that the minimal Scott–Vogelius method is higher order, with cubic velocities and discontinuous quadratic pressures on the Alfeld split, giving much lower error at the cost of a greater expense. Otherwise, the same relative rankings hold – Taylor–Hood and Alfeld–Sorokina may be the preferred choices based on the importance of the divergence-free condition.

We also give a basic estimate of the cost of the methods by measuring the number of floating-point operations (FLOPs) required to assemble the matrices in the system. The formulations (5.1) and (5.2) both lead to block matrices of the form

$$\begin{bmatrix} A & B^\top \\ B & 0 \end{bmatrix}, \quad (5.4)$$

where the matrices  $A$  and  $B$  differ between the pressure-velocity and stress-velocity formulations. In either case, both matrices are formed by iterating over cells to form local contributions and assembling them into the global sparse matrix. Fig. 11 gives the operation count reported by TSFC in the element-level kernels for  $A$  and  $B$ . These numbers assume that the reference basis functions are pre-tabulated but include the entire cost of forming Jacobians, transforming basis functions, and integrating over the cell. In each case, the cost of forming  $A$  greatly dominates that of  $B$ . We see that the non-macro nature of the Taylor–Hood pair makes assembly much cheaper than many of the alternatives. Note that, although the ISO element pair uses a macroelement velocity, it only uses piecewise linear polynomials on the splitting, and hence  $A$  requires only a single quadrature point on each subcell. Since total runtime typically depends more strongly on algebraic solvers than assembly, the relative advantages of macroelements may outweigh the increased assembly costs in many scenarios.

## 5.2 Navier-Stokes

We also applied our methods to a well-known benchmark for the two-dimensional Navier-Stokes equations, measuring the drag and lift on a cylinder and the pressure drop across it [John 2004; Schäfer et al. 1996]. The domain is given by  $\Omega = [0, 2.2] \times [0, 0.41] \setminus B_r(0.2, 0.2)$ , with radius  $r = 0.05$ , and is shown in Fig. 12. The density is taken as  $\rho = 1$  and kinematic viscosity is  $\nu = 10^{-3}$ , which gives a Reynolds number of 20. No-slip conditions are imposed on the top and bottom of the pipe and the cylinder. Natural boundary conditions (no-stress) are imposed on the outflow right end,



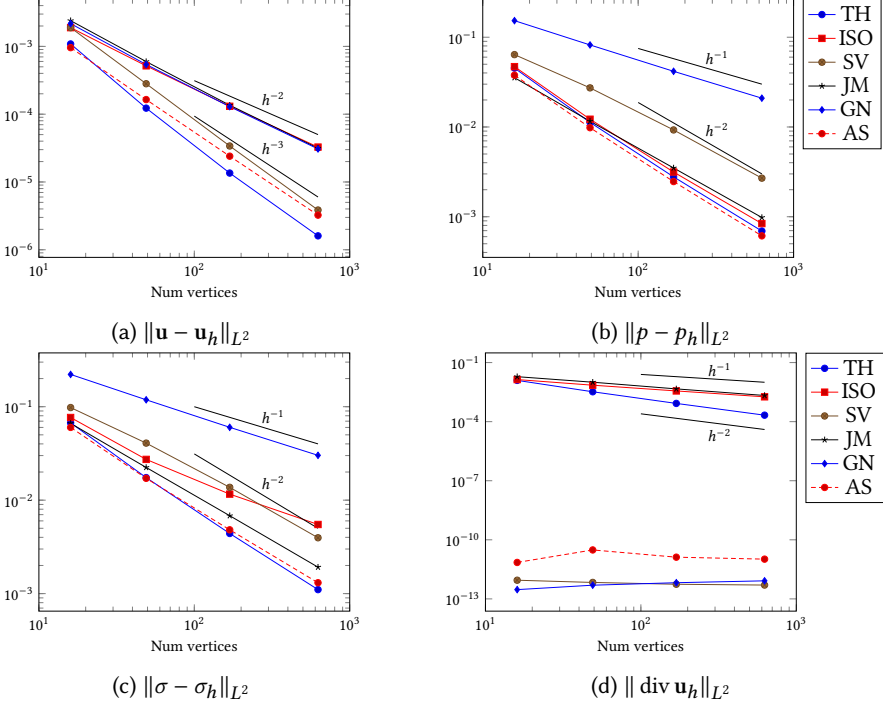


Fig. 9. Convergence under mesh refinement for various Stokes discretizations on an  $N \times N$  mesh of squares divided into right triangles. Taylor–Hood, Scott–Vogelius, reduced Arnold–Qin, and Alfeld–Sorokina use the velocity–pressure formulation (5.1), while Johnson–Mercier uses the stress–velocity formulation (5.2). Taylor–Hood elements are used on the original mesh, while the other formulations use macro–elements based on the Alfeld split.

and a parabolic profile is posed on the inflow boundary on the left end:

$$u(0, y) = \left( \frac{4y(0.41 - y)}{0.41^2}, 0 \right) \equiv U_{\text{in}}(y). \quad (5.5)$$

Fig. 13 shows the error in several key quantities as a function of mesh refinement for each of the methods considered for Stokes flow. These quantities are the lift and drag on the cylinder and the difference in the computed pressure  $p(0.15, 0.2) - p(0.25, 0.2)$  across the cylinder. These values are known to high accuracy [Nabh 1998]. We also report the computed norm of the divergence of the velocity per (5.3).

Perhaps surprisingly, we obtain a different relative ordering of accuracy between the various methods than for the Stokes equations, and this varies depending on the quantity of interest. The Johnson–Mercier formulation gives the best drag approximation, and nearly the best results for lift and pressure drop. The Taylor–Hood pair is competitive (and nearly the best for drag), but neither is it divergence free. Among the divergence-free methods, we see that Scott–Vogelius and Alfeld–Sorokina pairs are more accurate than the lower-order Guzman–Neilan pair. That each problem and functional may be best resolved by a different element (and even variational formulation) supports our goal of enabling a quite broad class of discretizations in the Firedrake code stack.

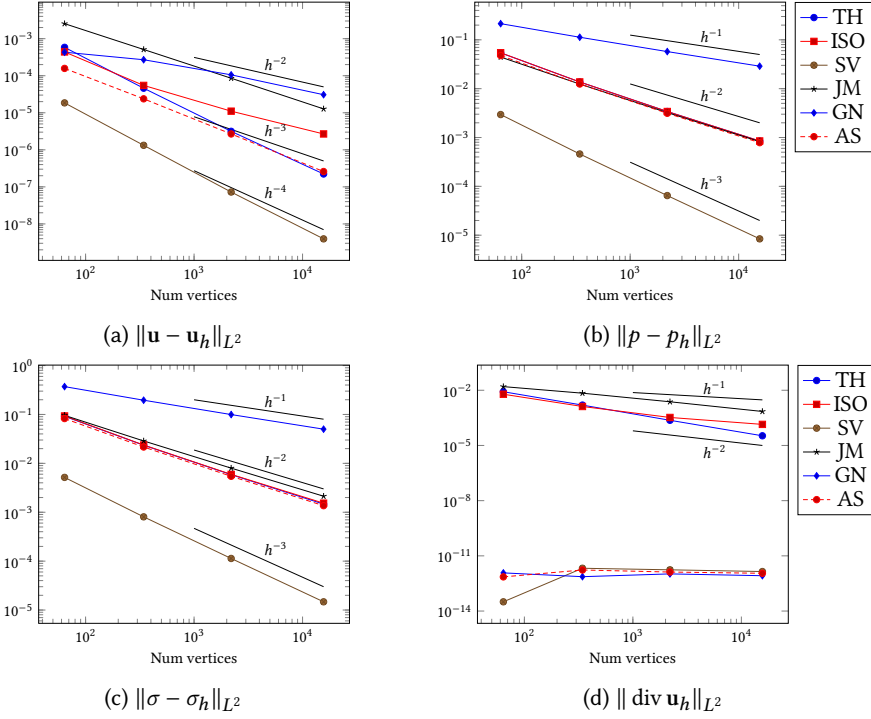


Fig. 10. Convergence under mesh refinement for various Stokes discretizations on an  $N \times N \times N$  mesh of cubes divided into six tetrahedra. Taylor–Hood and Scott–Vogelius use the velocity–pressure formulation (5.1), while Johnson–Mercier uses the stress–velocity formulation (5.2). Taylor–Hood elements are used on the original mesh, while the other formulations use macro–elements based on the Alfeld split.

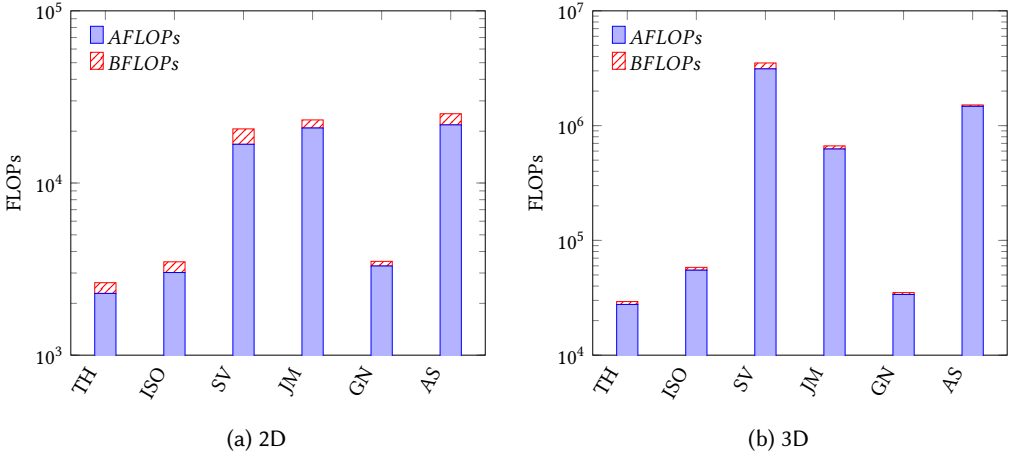


Fig. 11. FLOP count for evaluating the element–level kernels for the Stokes operator. This count assumes reference basis elements are pre–tabulated and then includes the cost of transforming basis functions and their derivatives and performing integration.

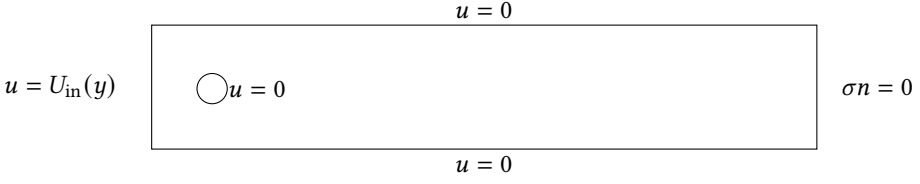


Fig. 12. Computational domain for flow past cylinder, with boundary conditions indicated on each part of the boundary.

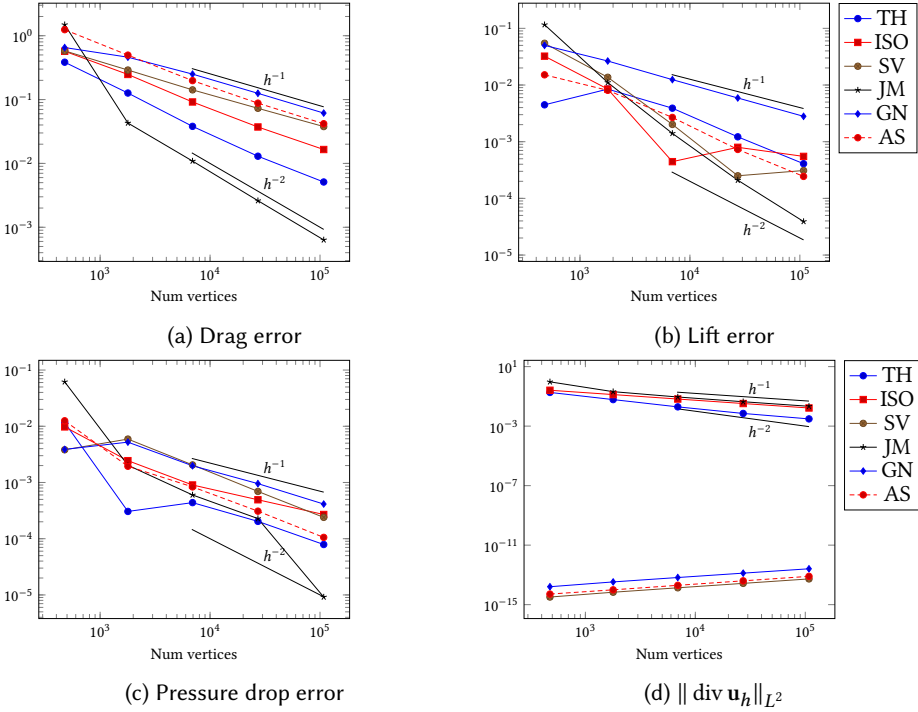


Fig. 13. Comparing the drag, lift, and pressure drop to reference values for for the 2d cylinder problem. The  $L^2$  norm the divergence is also included. Here, the Johnson–Mercier discretization of the stress-velocity formulation outperforms the Taylor–Hood and Scott–Vogelius discretization of the velocity-pressure formulation on each refinement level.

### 5.3 Fourth-order problems

Next, we apply our newly-enabled  $C^1$  macroelements to the plate-bending biharmonic problem,

$$\Delta^2 u = f \tag{5.6}$$

on  $\Omega$ . In our examples, we consider clamped boundary conditions  $u = \frac{\partial u}{\partial n} = 0$  on  $\partial\Omega$ . Following Brenner and Scott [2008], we employ the bilinear form

$$a(u, v) = \int_{\Omega} \Delta u \Delta v - (1 - \nu) (2u_{xx}v_{yy} + 2u_{yy}v_{xx} - 4u_{xy}v_{xy}) \, dx, \tag{5.7}$$

where  $0 \leq \nu \leq \frac{1}{2}$  is the plate's Poisson ratio. The terms multiplied by  $(1 - \nu)$  may separately be integrated by parts to give  $u_{xx}yyv$  times zero plus terms for incorporating strongly-supported boundary conditions. Subject to clamped boundary conditions, or on any subspace of  $H^2$  not containing linear polynomials over  $\Omega$ , the bilinear form  $a$  is coercive.

We used this example to validate our implementation of Morley, Argyris, and Bell elements in [Kirby and Mitchell 2019], and we repeat this experiment to include the newly-implemented HCT macroelement and its reduced variant. Macroelements facilitate the strong enforcement of the clamped boundary conditions, in contrast with [Kirby and Mitchell 2019], where the supersmooth elements with second derivative nodes required us to enhance the bilinear form with Nitsche-type terms. However, other choices of boundary conditions (for example  $u = 0 = \frac{\partial^2 u}{\partial n^2}$ ) might still require a Nitsche-type approach.

Fig. 14 plots the error versus mesh refinement, where we take a coarse mesh of the unit square, slightly perturb the internal vertices, and then take uniform refinements. Here, we see the HCT and its higher order variants provide more accurate results than the lower-order.

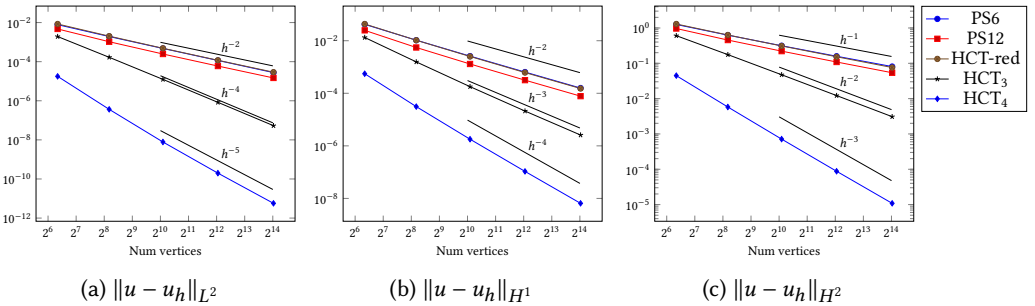


Fig. 14. Error in solving biharmonic equation on a perturbed  $N \times N$  mesh.

The macroelements give lower orders of accuracy, but have fewer global degrees of freedom and lower polynomial degree than the Bell and Argyris elements. However, because they use piecewise polynomials, we must integrate over each subcell, so it is also interesting to compare the work required to form each local stiffness matrix. Since reference element values are precomputed, this cost is not included, but the cost of forming element Jacobians, transforming the basis functions, and integrating are all computed. Fig. 15 shows the reported FLOP counts for these elements, comparing against some classical non-macro elements (the quadratic Morley element, plus Bell and two degrees of Argyris). The Powell-Sabin and cubic HCT elements indeed give a middle ground between the inexpensive but low-order Morley element and the higher-order polynomial  $C^1$  elements. We note that the HCT<sub>4</sub> element is actually more expensive than the Bell and quintic Argyris elements. Although the quintic Argyris element is more accurate and slightly lower-cost than the HCT<sub>4</sub> element, we note that some applications may benefit from the lack of higher derivatives at the vertices.

## 6 CONCLUSIONS AND FUTURE WORK

Here, we have developed a robust, general framework for the construction of reference bases for macroelements in FIAT and their integration into Firedrake. This appears to be the first such general-purpose implementation, and we are able to evaluate a representative suite of classical and modern elements for incompressible flow and biharmonic problems. At the same time, these results suggest the need for much ongoing work. For one, inter-grid transfers to enable multigrid

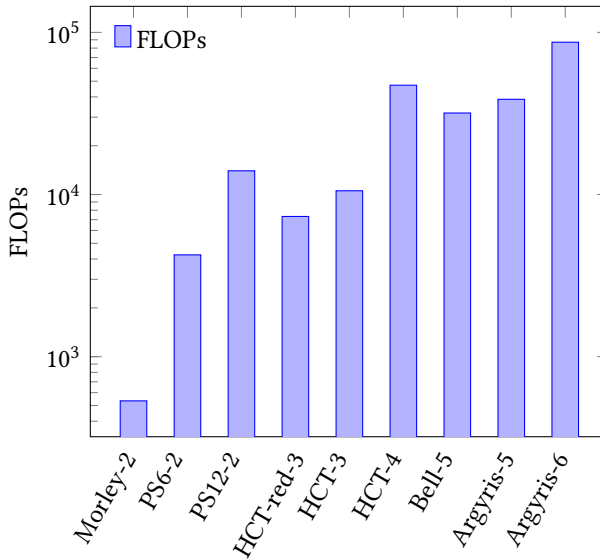


Fig. 15. FLOP count for evaluating the element-level kernel for the biharmonic operator. This count assumes reference basis elements are pre-tabulated and then includes the cost of transforming basis functions and their derivatives and performing integration.

algorithms for macroelement spaces are not fully understood, with mathematical and practical questions remaining. Also, optimizing element-level calculation for macroelements, whether by use of sparse arrays or iterating over subcells with indirection, remains an open issue. Finally, Firedrake supports sum-factorization of matrix-vector products on tensor product domains [Homolya et al. 2017], and combining this with 1D ISO-type macroelements for preconditioning as in [Pazner et al. 2023] should be possible in a quite general setting.

## A REPRODUCIBILITY

The exact version of Firedrake used, along with scripts employed for the generation of numerical data is archived on Zenodo [Brubeck and Kirby 2025].

## REFERENCES

- Mark Ainsworth, Gaelle Andriamaro, and Oleg Davydov. 2011. Bernstein–Bézier finite elements of arbitrary order and optimal assembly procedures. *SIAM Journal on Scientific Computing* 33, 6 (2011), 3087–3109.
- Peter Alfeld and Tatyana Sorokina. 2016. Linear differential operators on bivariate spline spaces and spline vector fields. *BIT Numerical Mathematics* 56 (2016), 15–32. <https://doi.org/10.1007/s10543-015-0557-x>
- Douglas N. Arnold, Gerard Awanou, and Ragnar Winther. 2008. Finite elements for symmetric tensors in three dimensions. *Math. Comp.* 77, 263 (July 2008), 1229–1251. <https://doi.org/10.1090/S0025-5718-08-02071-1>
- Douglas N. Arnold, Gerard Awanou, and Ragnar Winther. 2014. Nonconforming tetrahedral mixed finite elements for elasticity. *Mathematical Models and Methods in Applied Sciences* 24, 04 (2014), 783–796. <https://doi.org/10.1142/s021820251350067x>
- Douglas N. Arnold and Jinshui Qin. 1992. Quadratic velocity/linear pressure Stokes elements. *Advances in computer methods for partial differential equations* 7 (1992), 28–34.
- Douglas N. Arnold and Ragnar Winther. 2002. Mixed finite elements for elasticity. *Numer. Math.* 92, 3 (Sept. 2002), 401–419. <https://doi.org/10.1007/s002110100348>
- Douglas N. Arnold and Ragnar Winther. 2003. Nonconforming mixed elements for elasticity. *Mathematical Models and Methods in Applied Sciences* 13, 03 (March 2003), 295–307. <https://doi.org/10.1142/s0218202503002507>

- Francis R. A. Aznaran, Patrick E. Farrell, and Robert C. Kirby. 2022. Transformations for Piola-mapped elements. *The SMAI Journal of computational mathematics* 8 (2022), 399–437. <https://doi.org/10.5802/smai-jcm.91> arXiv:2110.13224 [math.NA]
- Christine Bernardi and Genevievè Raugel. 1985. Analysis of some finite elements for the Stokes problem. *Math. Comp.* 44 (1985), 71–79. <https://doi.org/10.1090/S0025-5718-1985-0771031-7>
- Andreas Bock, Colin J. Cotter, and Robert C. Kirby. 2024. Planar curve registration using Bayesian inversion. *Computers & Mathematics with Applications* 159 (2024), 155–172. <https://doi.org/10.1016/j.camwa.2024.02.005> arXiv:2307.04909 [cs.CV]
- Susanne C. Brenner and L. Ridgway Scott. 2008. *The mathematical theory of finite element methods* (third ed.). Texts in Applied Mathematics, Vol. 15. Springer, New York. xviii+397 pages.
- Pablo D. Brubeck and Robert C. Kirby. 2025. Software used in ‘FIAT: enabling classical and modern macroelements’. <https://doi.org/10.5281/zenodo.14733364>
- Pablo D. Brubeck, Robert C. Kirby, Fabian Laakmann, and Lawrence Mitchell. 2024. FIAT: improving performance and accuracy for high-order finite elements. *arXiv:2403.13189* (2024).
- Carsten Carstensen, Joscha Gedicke, and Eun-Jae Park. 2012. Numerical experiments for the Arnold–Winther mixed finite elements for the Stokes problem. *SIAM Journal on Scientific Computing* 34, 4 (2012), A2267–A2287.
- Philippe G. Ciarlet. 2002. *The finite element method for elliptic problems*. SIAM.
- Ray W. Clough and J. L. Toucher. 1965. Finite element stiffness matrices for analysis of plate bending. In *Proc. of the First Conf. on Matrix Methods in Struct. Mech.* 515–546.
- Jay Gopalakrishnan, Johnny Guzman, and Jeonghun J. Lee. 2024. The Johnson-Mercier elasticity element in any dimensions. *arXiv preprint arXiv:2403.13189* (2024).
- Jay Gopalakrishnan, Philip L. Lederer, and Joachim Schöberl. 2020. A mass conserving mixed stress formulation for Stokes flow with weakly imposed stress symmetry. *SIAM J. Numer. Anal.* 58, 1 (2020), 706–732.
- Jan Grošelj and Marjeta Knez. 2022. Generalized  $C^1$  Clough–Tocher splines for CAGD and FEM. *Computer Methods in Applied Mechanics and Engineering* 395 (2022), 114983. <https://doi.org/10.1016/j.cma.2022.114983>
- Johnny Guzmán and Michael Neilan. 2018. Inf-sup stable finite elements on barycentric refinements producing divergence-free approximations in arbitrary dimensions. *SIAM J. Numer. Anal.* 56, 5 (2018), 2826–2844.
- David A. Ham, Paul H. J. Kelly, Lawrence Mitchell, Colin J. Cotter, Robert C. Kirby, Koki Sagiyama, Nacime Bouziani, Sophia Vorderwuelbecke, Thomas J. Gregory, Jack Betteridge, Daniel R. Shapero, Reuben W. Nixon-Hill, Connor J. Ward, Patrick E. Farrell, Pablo D. Brubeck, India Marsden, Thomas H. Gibson, Miklós Homolya, Tianjiao Sun, Andrew T. T. McRae, Fabio Luporini, Alastair Gregory, Michael Lange, Simon W. Funke, Florian Rathgeber, Gheorghe-Teodor Bercea, and Graham R. Markall. 2023. *Firedrake User Manual* (first ed.). Imperial College London and University of Oxford and Baylor University and University of Washington. <https://doi.org/10.25561/104839>
- F. Hecht. 2012. New development in FreeFem++. *J. Numer. Math.* 20, 3–4 (2012), 251–265. <https://freefem.org/>
- Miklós Homolya, Robert C. Kirby, and David A. Ham. 2017. Exposing and exploiting structure: optimal code generation for high-order finite element methods. arXiv:1711.02473 [cs.MS]
- Miklós Homolya, Lawrence Mitchell, Fabio Luporini, and David A. Ham. 2018. TSFC: a structure-preserving form compiler. *SIAM Journal on Scientific Computing* 40, 3 (2018), C401–C428.
- Volker John. 2004. Reference values for drag and lift of a two-dimensional time-dependent flow around a cylinder. *International Journal for Numerical Methods in Fluids* 44, 7 (2004), 777–788.
- Claes Johnson and Bertrand Mercier. 1978. Some equilibrium finite element methods for two-dimensional elasticity problems. *Numer. Math.* 30 (1978), 103–116.
- George Karniadakis and Spencer J. Sherwin. 2005. *Spectral/hp element methods for computational fluid dynamics*. Oxford University Press, USA.
- Robert C. Kirby. 2004. Algorithm 839: FIAT, a new paradigm for computing finite element basis functions. *ACM Trans. Math. Software* 30, 4 (2004), 502–516. <https://doi.org/10.1145/1039813.1039820>
- Robert C. Kirby. 2006. Optimizing FIAT with level 3 BLAS. *ACM Trans. Math. Software* 32, 2 (2006), 223–235. <https://doi.org/10.1145/1141885.1141889>
- Robert C. Kirby. 2010. Singularity-free evaluation of collapsed-coordinate orthogonal polynomials. *ACM Trans. Math. Software* 37, 1 (2010), 1–16. <https://doi.org/10.1145/1644001.1644006>
- Robert C. Kirby. 2011. Fast simplicial finite element algorithms using Bernstein polynomials. *Numer. Math.* 117, 4 (2011), 631–652.
- Robert C. Kirby. 2014. Low-complexity finite element algorithms for the de Rham complex on simplices. *SIAM Journal on Scientific Computing* 36, 2 (2014), A846–A868.
- Robert C. Kirby. 2018. A general approach to transforming finite elements. *SMAI Journal of Computational Mathematics* 4 (2018), 197–224. <https://doi.org/10.5802/smai-jcm.33>
- Robert C. Kirby and Anders Logg. 2006. A compiler for variational forms. *ACM Trans. Math. Software* 32, 3 (2006), 417–444.
- Robert C. Kirby and Lawrence Mitchell. 2019. Code generation for generally mapped finite elements. *ACM Trans. Math. Software* 45, 4 (2019), 41:1–41:23. <https://doi.org/10.1145/3361745> arXiv:1808.05513 [cs.MS]

- Ming-Jun Lai and Larry L. Schumaker. 2007. *Spline functions on triangulations*. Number 110. Cambridge University Press.
- Andrew T. T. McRae, Gheorghe-Teodor Bercea, Lawrence Mitchell, David A. Ham, and Colin J. Cotter. 2016. Automated generation and symbolic manipulation of tensor product finite elements. *SIAM Journal on Scientific Computing* 38, 5 (2016), S25–S47. <https://doi.org/10.1137/15M1021167> arXiv:1411.2940 [math.NA]
- Guido Nabh. 1998. *On High Order Methods for the Stationary Incompressible Navier–Stokes Equations*. Universität Heidelberg. Interdisziplinäres Zentrum für Wissenschaftliches Rechnen.
- Will Pazner, Tzanio Kolev, and Clark R Dohrmann. 2023. Low-order preconditioning for the high-order finite element de Rham complex. *SIAM Journal on Scientific Computing* 45, 2 (2023), A675–A702.
- Michael J. D. Powell and Malcolm A. Sabin. 1977. Piecewise quadratic approximations on triangles. *ACM Transactions on Mathematical Software (TOMS)* 3, 4 (1977), 316–325.
- Florian Rathgeber, David A. Ham, Lawrence Mitchell, Michael Lange, Fabio Luporini, Andrew T. T. McRae, Gheorghe-Teodor Bercea, Graham R. Markall, and Paul H. J. Kelly. 2016. Firedrake: automating the finite element method by composing abstractions. *ACM Trans. Math. Software* 43, 3 (2016), 24:1–24:27. <https://doi.org/10.1145/2998441> arXiv:1501.01809 [cs.MS]
- Yves Renard and Konstantinos Poullos. 2020. GetFEM: Automated FE modeling of multiphysics problems based on a generic weak form language. *ACM Trans. Math. Software* 47, 1 (2020), 1–31.
- Marie E. Rognes, Robert C. Kirby, and Anders Logg. 2010. Efficient assembly of  $H(\text{div})$  and  $H(\text{curl})$  conforming finite elements. *SIAM Journal on Scientific Computing* 31, 6 (2010), 4130–4151. <https://doi.org/10.1137/08073901X> arXiv:1205.3085 [math.NA]
- M. Schäfer, S. Turek, F. Durst, E. Krause, and R. Rannacher. 1996. *Benchmark Computations of Laminar Flow Around a Cylinder*. Vieweg+Teubner Verlag, Wiesbaden, 547–566. [https://doi.org/10.1007/978-3-322-89849-4\\_39](https://doi.org/10.1007/978-3-322-89849-4_39)
- L. Ridgway Scott and Micheal Vogelius. 1984. *Conforming Finite Element Methods for Incompressible and Nearly Incompressible Continua*. Technical Report. Maryland Univ. College Park Inst. For Physical Science And Technology.
- Matthew W. Scroggs, Igor A. Baratta, Chris N. Richardson, and Garth N. Wells. 2022. Basix: a runtime finite element basis evaluation library. *Journal of Open Source Software* 7, 73 (2022), 3982. <https://doi.org/10.21105/joss.03982>
- Roy H. Stogner and Graham F. Carey. 2007.  $C^1$  macroelements in adaptive finite element methods. *Internat. J. Numer. Methods Engrg.* 70, 9 (2007), 1076–1095.
- Andrew J. Worsey and B. Piper. 1988. A trivariate Powell-Sabin interpolant. *Computer Aided Geometric Design* 5, 3 (1988), 177–186.
- Hong Xiao and Zydrunas Gimbutas. 2010. A numerical algorithm for the construction of efficient quadrature rules in two and higher dimensions. *Computers & Mathematics with Applications* 59, 2 (2010), 663–676. <https://doi.org/10.1016/j.camwa.2009.10.027>